

Global Particle Simulation Study of Substorm Onset and Particle Acceleration

Ken-Ichi Nishikawa (kenichi@physics.rutgers.edu)

Department of Physics and Astronomy, Rutgers, The State University of New Jersey, 136 Frelinghuysen Road, Piscataway, NJ 08854-8019

March 8, 2000

Abstract. This paper reports the spatial and temporal development of Bursty Bulk Flows (BBFs) created by the reconnection as well as current disruptions (CDs) in the near-Earth tail using our 3-D global EM particle simulation with a southward turning IMF in the context of the substorm onset. Recently, observations show that BBFs are often accompanied by current disruptions for triggering substorms. We have examined the dynamics of BBFs and CDs in order to understand the timing and triggering mechanism of substorms. As the solar wind with the southward IMF advances over the Earth, the near-Earth tail thins and the sheet current intensifies. Before the peak of the current density becomes maximum, the reconnection takes place, which ejects particles from the reconnection region. Because of the earthward flows the peak of the current density moves toward the Earth. The characteristics of the earthward flows depend on the ions and electrons. Electrons flow back into the inflow region (the center of reconnection region), which provides current closure. Therefore the structure of electron flows near the reconnection region is rather complicated. In contrast, the ion earthward flows are generated far from the reconnection region. These earthward flows pile up near the Earth. The ions mainly drift toward the duskside. The electrons are diverted toward the dawnside. Due to the pile-up, dawnward current is generated near the Earth. This dawnward current dissipates rapidly with the sheet current because of the opposite current direction, which coincides with the dipolarization in the near-Earth tail. At this time the wedge current may be created in our simulation model. This simulation study shows the sequence of the substorm dynamics in the near-Earth tail, which is similar to the features obtained by the multisatellite observations. The identification of the timing and mechanism of triggering substorm onset requires further studies in conjunction with observations.

Keywords: magnetic reconnection, Bursty Bulk Flows, flow braking, current disruption, field-aligned currents, substorms, particle acceleration

1. Introduction

In this study, which combines 3-D EM particle simulations and observations, the substorm onset is investigated with the synergetic effects among Near-Earth Neutral Line (NENL) (reconnection), current disruption and flow braking models.

Recently observations show BBFs are accompanied by substorm onsets (Sergeev et al., 1995, 1999; Angelopoulos et al., 1992, 1999;



© 2000 Kluwer Academic Publishers. Printed in the Netherlands.

Nagai et al., 1998; Mukai et al., 1998; Ohtani et al., 1998, 1999). These high-velocity plasma flows lead to the braking in the near-Earth region (Haerendel, 1992; Shiokawa et al., 1997, 1998a, b; Birn and Hesse, 1996; Birn et al., 1999; Baumjohann et al., 1990, 1999). Recently, Lui et al. (1999) found that the observations are inconsistent with the idea that the dipolarization is an MHD process of magnetic flux pile-up from braking of sunward plasma flow. Current disruption instabilities serve as the mesoscale or microscale internal processes to facilitate the transition from a tail-like to dipole-like field configuration in the plasma sheet (e.g., Lui, 1991; 1996). The new conjecture suggests that the near-Earth magnetotail is an important region for the substorm trigger (Mukai et al., 1998; Ohtani et al., 1998, 1999, and references therein).

On the basis of this idea we have investigated the temporal and spatial evolution of the near-Earth magnetotail in order to study the substorm onset with emphasis on the cause-and-effect relationship among the formation of a near-Earth neutral line (NENL) (e.g., Baker et al., 1999), earthward plasma flows, flow braking, and current disruption.

In this report the temporal and spatial evolution of the ion and electron earthward flows is studied systematically as well as their flow braking near the Earth. This simulation study shows the sequence of the substorm dynamics in the near-Earth tail. The identification of the timing and mechanism of triggering substorm onset has been attempted with the present model. In section 2 we describe new findings with the earthward plasma flows. The concluding remarks and future studies are discussed in section 3.

2. Simulation Models and Results

The increase of available core memory and speed on supercomputers such as the CRAY C90 and T90 now enables us to perform 3-D particle simulations with reasonably realistic parameters. We use a 3-D electromagnetic particle code (Buneman, 1993). This code utilizes charge-conserving formulas (Villasenor and Buneman, 1992) and radiating boundary conditions (Lindman, 1975). Due to space limitations, please refer to (Nishikawa 1997, 1998a, b; Nishikawa and Ohtani, 2000) for the initial and boundary conditions and parameters used in our simulations. (The simulation grid Δ corresponds to approximately $1R_E$. The time step in our simulation may be estimated as about 10 seconds on the basis of the solar wind velocity and the mass ratio used.) Time step 1152 in our simulation is set at 0.00 UT in order to provide a sense of realistic time frame (1216: 00.10UT; 1280: 00.20UT; 1344: 00.30UT; 1408: 00.40UT; 1472: 00.50UT).

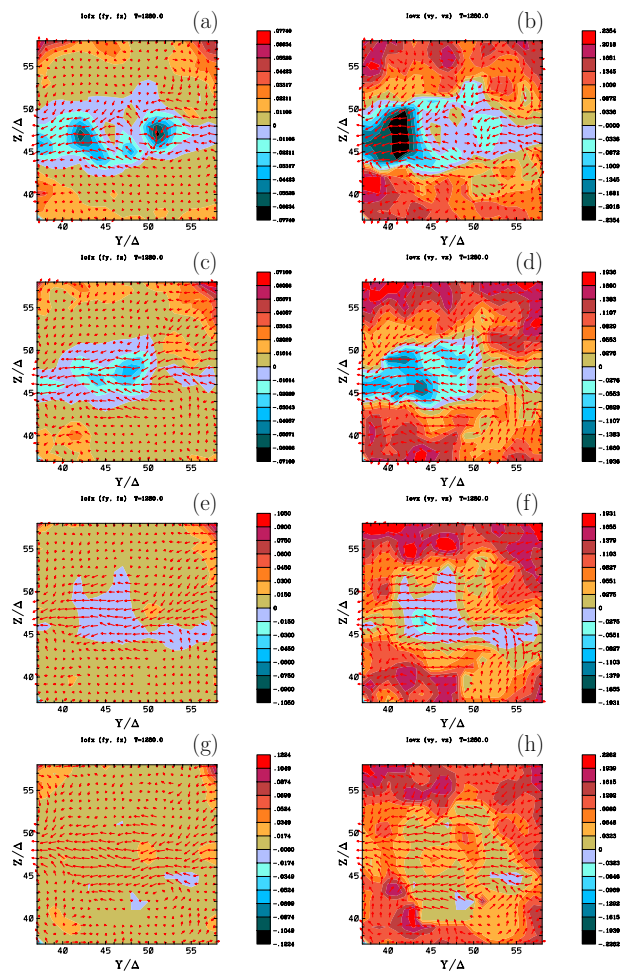


Figure 1. Ion flux (a, c, e, and g) and velocity (b, d, f, and h) on the dusk-dawn cross-section plane at $x = -8R_E$ (a and b), $-10R_E$ (c and d), $-12R_E$ (e and f), and $-14R_E$ (g and h) at 0.20UT (1280). The arrows show the ion flux (a, c, e, and g) and ion velocity (b, d, f, and h) on the plane (rescaled to show small values).

In order to study the dynamics of the earthward plasma flows generated by the reconnection, flux (left column) and velocity (right column) in the plasma sheet ($45\Delta < z < 51\Delta$) and the north and south lobes (outside the plasma sheet) are plotted at 0.20UT (1280) after the reconnection takes place (Figure 1: ion; Figure 2: electron). The flux and velocity are calculated by $f_x = \sum v_x(i)$ and $v_x = \sum v_x(i) / \sum i$, respectively. Figure 1 shows the ion flux and velocity in the dusk-dawn cross section plane at $x = -8R_E$ (a and b), $-10R_E$ (c and d), $-12R_E$

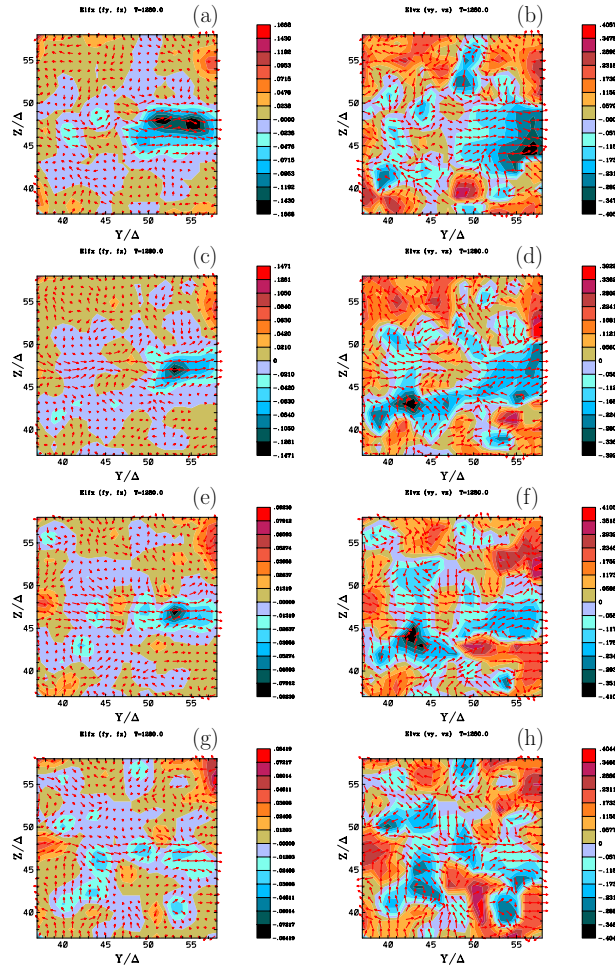


Figure 2. Electron flux (a, c, e, and g) and velocity (b, d, f, and h) on the dusk-dawn cross-section plane at $x = -8R_E$ (a and b), $-10R_E$ (c and d), $-12R_E$ (e and f), and $-14R_E$ (g and h) at 0.20UT (1280). The arrows show the electron flux (a, c, e, and g) and electron velocity (b, d, f, and h) on the plane (rescaled to show small values).

(e and f), and $-14R_E$ (g, and h). (The plots are viewed from the tail toward the Sun and the Earth is located at $x = 70.5\Delta$, $y = 47.5\Delta$, $z = 48\Delta$.) Ions are drifting mainly toward the dusk as shown by arrows. The earthward ion flux (blues) increases near the Earth $x = -8R_E$ (Fig. 1a). The earthward high velocity (blues) is seen in the duskside as shown in Fig. 1b. The maximum earthward velocity is approximately 4.7 times higher than the ion thermal velocity in the solar wind (about 94% of the solar wind velocity). The earthward ion high flux and high

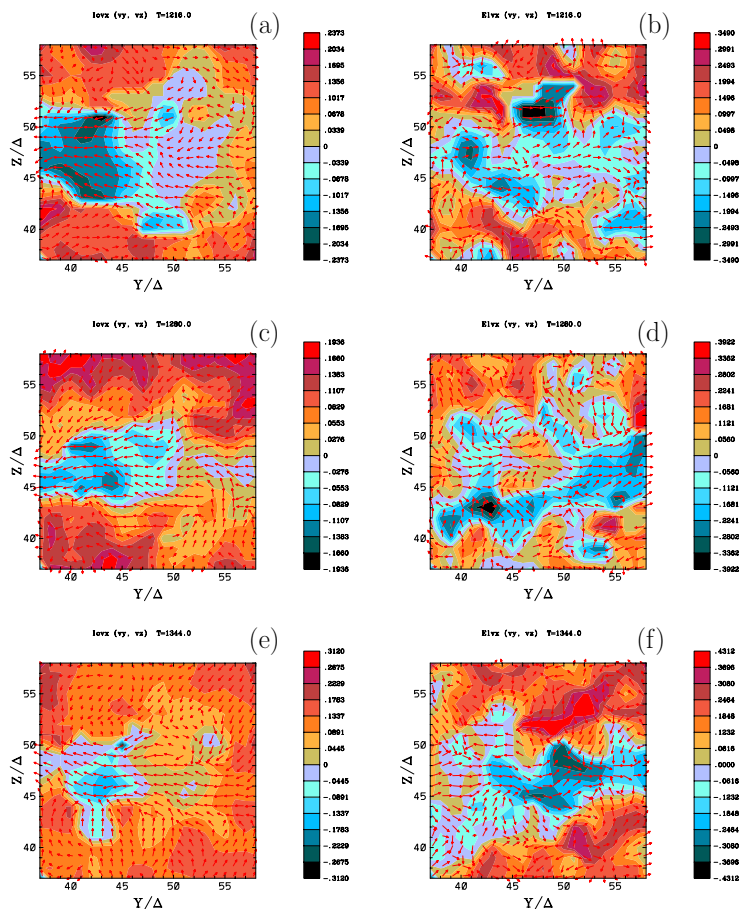


Figure 3. Evolution of ion (a, c, and e) and electron (b, d, and f) velocities on the dusk-dawn cross section plane at $x = -10R_E$ at 0.10UT (1216) (a and b), 0.20UT (1280) (c and d), and 0.30UT (1344) (e and f). The arrows show the ion (a, c, and e) and electron (b, d, and f) velocities on the plane (rescaled to show small values).

velocity are confined to the plasma sheet (Fig. 1a, 1b, 1c, and 1d). The rather high-velocity tailward flows (reds) are found in the lobe (near the mantle) (Fig. 1b, 1d, 1f, and 1h). Figure 2 shows electron flux and velocity at the same time. In contrast to the ion earthward fluxes, earthward electron fluxes are found near the reconnection region ($x \approx -15R_E$) as shown in Fig. 2g. It should be noted that the tailward flux is mixed with the earthward flux, which indicates the generation of current closure near the null points (the 3-dimensional reconnection) (Cai and Nishikawa, 1999) (more complicated than the X point in the 2-dimensional simulation) (Sonnerup, 1979; Terasawa, 1983). High

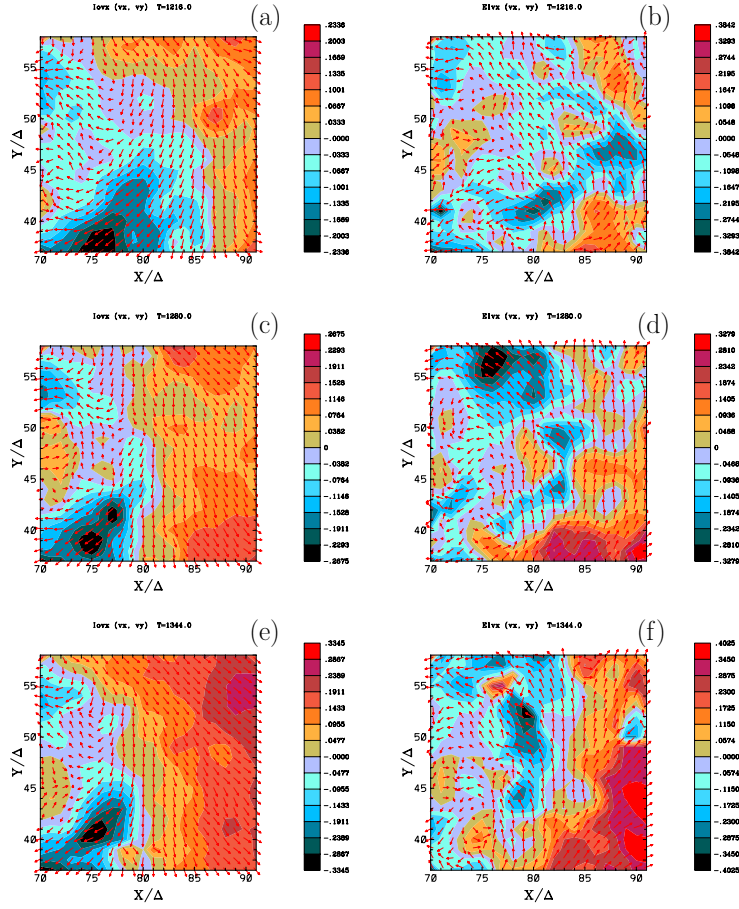


Figure 4. Evolution of ion (a, c, and e) and electron (b, d, and f) velocities (v_x) in the equatorial plane ($z = 48\Delta$) at 0.10UT (1216) (a and b), 0.20UT (1280) (c and d), and 0.30UT (1344) (e and f). The arrows show the ion (a, c, and e) and electron (b, d, and f) velocities ($v_{x,y}$) on the plane (rescaled to show small values).

earthward electron flux is confined to the plasma sheet, however, earthward high velocity electrons are found in the outside of the central plasma sheet, since electrons are accelerated along the magnetic separatrices. The earthward high electron flux is found in the dawnside (near the Earth) at $x = -8R_E$ (Fig. 2b). Electrons are diverted mainly toward the dawn as expected. The highest earthward electron velocity reaches about 4 times the electron thermal velocity in the solar wind (about 150% of the solar wind velocity). Because of the small number of particles in the tail (especially, in the lobes) additional heating (acceleration) caused by large fluctuations may also be included together

with the acceleration by the reconnection. (The simulations with more particles in the cell are in progress in order to reduce fluctuations.)

On the basis of the simulation results the local reconnection start to take place at 0.10UT (1216). The time evolution of ion and electron velocity in the dusk-dawn cross section plane at $x = -10R_E$ is plotted in Figure 3. The earthward high ion velocity (blues) in the dawnside at 0.10UT (1216) (Fig. 3a) decreases at later time (Fig. 3c and 3e). In contrast, earthward high velocity electrons remain almost the same at later time as shown in Fig. 3b, 3d, and 3f. At later time (0.30UT) (1344) the earthward high velocity electrons are localized in the plasma sheet (Fig. 3f).

The main processes that generate the wedge current take place near the Earth. (The Earth is located at $x = 70.5\Delta$, $y = 47.5\Delta$.) In order to examine the flow diversion and current disruption, the ion and electron velocities (the v_x : color, $v_{x,y}$: arrows) are plotted in the equatorial plane (Figure 4). Ions are mainly diverted toward the dusk (Fig. 4a, 4c, and 4e), and electrons are diverted toward the dawn (Fig. 4b, 4d, and 4f). On the basis of ion and electron velocity structures in the tail, their high velocity flows are localized and transient. In order to examine the effects of current disruptions, the electron velocity in the equatorial plane has been examined, since electrons are easily affected with turbulent electromagnetic fields caused by the cross-field current instability (CCI) (Lui, 1991, 1996). As shown in electron velocity structures (in the right column), near the Earth (within $10R_E$) the electron velocities look irregular because of the turbulence, which supports an evidence of occurrence of CCI (see also Figs. 3b, 3d, 3f, 5c, and 5d).

The dipolarization is one of the processes that is closely related to the wedge current (e.g., Kan, 1998; Ohtani et al., 1999). Observations show that current disruption and flow braking are accompanied by dipolarization. Figure 5 shows the differences of the B_z in the equatorial plane from that at 0.00UT (1152) when the southward IMF effects are not visible yet (Fig. 5a). (The strong negative magnetic field in the Earth is truncated at -50 .) At 0.10UT (1216) the B_z decreases near the Earth shown by blues (Fig. 5b). At this time the B_z becomes negative locally and the local null points are found in the duskside near-Earth tail (Cai and Nishikawa, 1999). The reconnection takes place between time 0.10 - 0.20UT (1216 and 1280). As shown in Fig. 5c the B_z decreases in the entire region. At 0.30UT (1344) the B_z increases locally near the Earth shown by reds, which shows the dipolarization. The dipolarization is more visible in the dawnside as shown in Fig. 5d, 5e, and 5f. After the reconnection, the dipolarization takes place near the Earth at 0.30UT (1344) as shown in Fig. 5d. The arrows show the

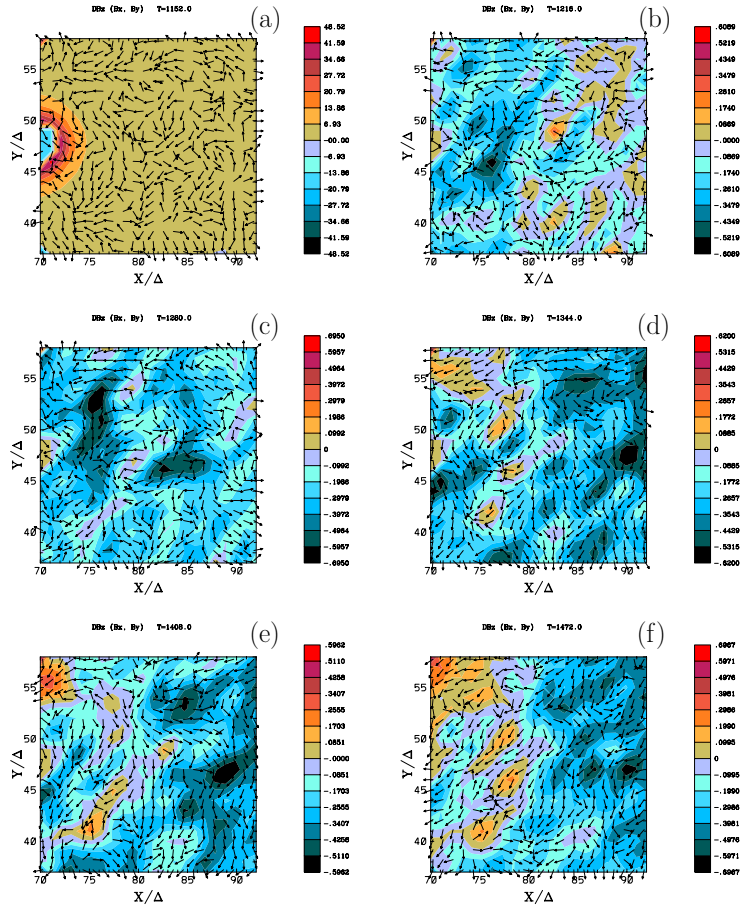


Figure 5. Time evolution of the B_z magnetic field component subtracted by the value at 0.00UT (1152) (a) in the equatorial ($x-y$) plane ($z = 48\Delta$) near the Earth magnetosphere at 0.10UT (1216) (b), 0.20UT (1280) (c), 0.30UT (1344) (d), 0.40UT (1408) (e), and 0.50UT (1472) (f). The arrows show the magnetic field ($B_{x,y}$) in the equatorial plane.

magnetic field components (B_x , B_y) in the equatorial plane. The complex magnetic structure supports an evidence of turbulence caused by the CCI (current disruption). As shown in Figure 1 in (Nishikawa and Ohtani, 2000), the current density on the subsolar line at $x = 79 (\approx -9R_E)$ becomes maximum at 0.10UT (1216) and decreases at 0.30UT (1344) (by about one third), which indicates the occurrence of current decrease (disruption).

3. Discussion

The evolution of near-Earth tail with a southward turning IMF is studied in order to address the cause-and-effect relationship between the reconnection, BBFs, flow braking, and current disruption. The southward IMF drives the sequence of processes which lead to the substorm onset in the near-Earth magnetotail as shown in the previous section. Our 3-D global EM particle simulation results show that the cross-field current is enhanced at the substorm growth phase with a southward IMF. The duskward electric field accompanied by the southward IMF begins to enhance the current sheet in the near-Earth magnetotail. The current sheet is thinned, and at the same time the local reconnection takes place (Cai and Nishikawa, 1999). Later the (full) reconnection takes place and ejects particles, which generates (high-velocity) ion and electron flows in the near-Earth tail as shown in Figures 1 - 4. The dawnward current is generated by the braking of earthward flows. Due to the dawnward current the gradient of current density near the Earth ($-5R_E > x > -8R_E$) becomes very steep at 0.20UT (1280). Because of the opposite current direction between the dawnward current and the cross-field current they decrease rapidly with the dipolarization as shown in Figure 5d. On the basis of these simulation results we infer that the current disruption plays a role in triggering substorm onset in assistance with the flow braking of earthward flows generated by the reconnection.

The field-aligned current at $r = 5R_E$ on the north pole is examined in order to check the validity of the present simplest ionospheric response in which particles are reflected by the mirror force in the cusps. (The parallel current is calculated by $j_{\parallel} = \mathbf{J} \cdot \mathbf{B} / |\mathbf{B}|$.) This ionospheric model includes the ambipolar field and effects of gyromotion in the dipole magnetic field near the Earth (grad-B/curvature currents). Figure 6 shows the time evolution of field-aligned currents (FACs) which are projected on the equatorial plane. (The outer regions are shrunk.) These circular areas contain about 50 original simulation square grids. The figures are plotted with 16 times better resolutions by the interpolations. The inward (into the ionosphere) current is shown by blues and outward (tailward) currents are plotted by reds. The upper side is faced toward the Sun and the right side is faced toward the dawn. The latitude ranges from 90° to 37° . The current in the region outside the radius $4R_E$ (on the equatorial plane) is set at zero. As expected at least a pair of inward and outward currents is found. The intensity of current is not changed except at 0.40UT (1408). At 0.30UT (1344) (Figure 6c) two pairs of currents are found with the dipolarization (see Fig. 5c) and this current pattern is consistent with a schematic diagram of

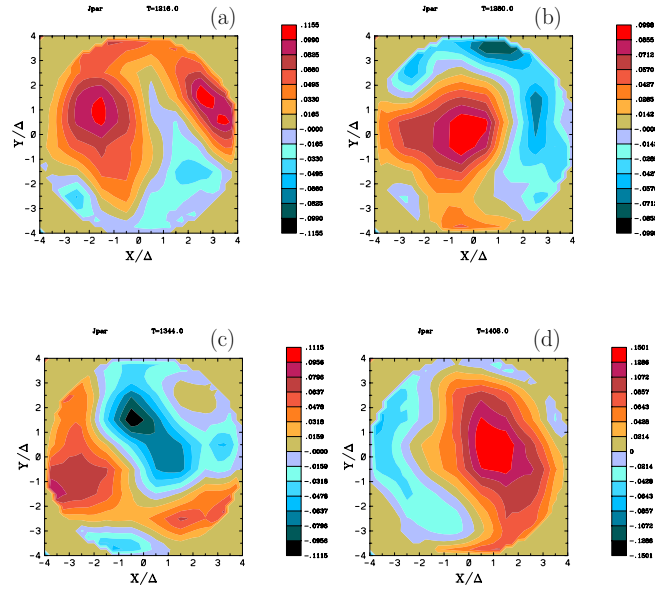


Figure 6. Time evolution of the field-aligned current at $r = 5\Delta (\approx 5R_E)$ around the north pole ($90^\circ - 36.9^\circ$) (projected on the equatorial plane and viewed from the pole) at 0.10UT (1216) (a), 0.20UT (1280) (b), 0.30UT (1344) (c), and 0.40UT (1408) (d). The inward and outward currents are shown by blues and reds, respectively.

field-aligned current shown in Plate 4 in (Birn et al., 1999). The pair with a stronger current near the pole may correspond to the region I current and another pair with a weaker current in the nightside may correspond to the region II current. However, this current pattern is different from the observed distribution of upward and downward field-aligned currents in invariant latitude-MLT coordinate (Iijima and Potemra, 1978). This comes from the fact that the resolutions near the Earth are coarse and ionospheric conductivities may not be included correctly in our simulations. The current structure at 0.40UT (1408) seems to correspond to the region II current. In order to examine the FACs obtained by our simulations, the question how FACs are closed at the inner boundary (at the ionosphere ($r \approx 2R_E$)) needs to be answered. We also need to improve the ionospheric model in our simulations including the ionospheric dynamics such as ionospheric outflows. (The color figures are viewed at <http://www.physics.rutgers.edu/~kenichi>.)

Acknowledgements

The author thanks S. Ohtani, and A. T. Y Lui for fruitful comments. Support for this work was provided by NSF grants ATM-9730230 and

ATM-9996266. The development of the simulation code was performed at the National Center for Supercomputing Applications, University of Illinois at Urbana-Champaign, and the production runs were performed at Pittsburgh Supercomputing Center. The postanalysis of simulations has been made at San Diego Supercomputing Center. All centers are supported by the National Science Foundation.

References

- V. Angelopoulos, W. Baumjohann, C. F. Kennel, F. V. Coroniti, M. G. Kivelson, R. Pellat, R. J. Walker, H. Lühr, and G. Paschmann. Bursty bulk flows in the inner central plasma sheet, *J. Geophys. Res.*, 97:4027, 1992.
- V. Angelopoulos, F. S. Mozer, T. Mukai, K. Tsuruda, S. Kokubun, and T. J. Hughes. On the relationship between bursty flows, current disruption and substorms, *Geophys. Res. Lett.* 16:2841, 1999.
- D. N. Baker, T. I. Pukkinen, J. Büner, and A. J. Klimas, Substorms: A global instability of the magnetosphere-ionosphere system, *J. Geophys. Res.*, 104:14,601, 1999.
- W. Baumjohann, G. Paschmann, and H. Lühr, Characteristics of high-speed ion flows in the plasma sheet, *J. Geophys. Res.*, 95:3801, 1990.
- W. Baumjohann, M. Hesse, S. Kokubun, T. Mukai, T. Nagai, and A. A. Petrukovich, Substorm dipolarization and recovery, *J. Geophys. Res.*, 104:24,995, 1999.
- J. Birn, and M. Hesse, Details of current disruption and diversion in simulations of magnetotail dynamics, *J. Geophys. Res.*, 101:15,345, 1996.
- J. Birn, M. Hesse, G. Haerendel, W. Baumjohann, and K. Shiokawa, Flow braking and the substorm current wedge, *J. Geophys. Res.*, 104:19,905, 1999.
- O. Buneman, TRISTAN: The 3-D E-M Particle Code, in *Computer Space Plasma Physics: Simulation Techniques and Software*, edited by H. Matsumoto and Y. Omura, P. 67, Terra Sci., Tokyo, 1993.
- D.-S. Cai, and K.-I. Nishikawa, Topological magnetic structure related to reconnection in the near-Earth magnetotail with southward IMF studied by three-dimensional electromagnetic particle code, *Geophys. Res. Lett.*, submitted, 1999.
- G. Haerendel, Disruption, ballooning, or auroral avalanche: On the cause of substorms. in *Proc. 1st Intl. Conf. Substorms (ICS-1)*, Kiruna, Sweden, p. 417, ESA, 1992.
- T. Iijima, and T. A. Potemra, Large-scale characteristic of field-aligned current, *J. Geophys. Res.*, 83:599, 1978.
- R. L. Kaufmann, Substorm currents: Growth phase and onset, *J. Geophys. Res.*, 92:7471, 1987.
- J. R. Kan, A globally integrated substorm model: Tail reconnection and magnetosphere-ionosphere coupling, *J. Geophys. Res.*, 103:11,787, 1998.
- E. L. Lindman, Free-space" boundary conditions for the time dependent wave equation, *J. Comput. Phys.*, 18:66, 1975.
- A. T. Y. Lui, A synthesis of magnetospheric substorm models, *J. Geophys. Res.*, 96:1849, 1991.
- A. T. Y. Lui, Current disruption in the Earth's magnetosphere: Observations and models, *J. Geophys. Res.*, 101:13,067, 1996.

- A. T. Y. Lui, K. Liou, M. Nosé, S. Ohtani, D. J. Williams, T. Mukai, T. Tsuruda, and S. Kokubun, Near-earth dipolarization: Evidence for a non-MHD process, *Geophys. Res. Lett.*, 26:2905, 1999.
- T. Mukai, M. Hoshino, Y. Saito, I. Shinohara, and T. Yamamoto, Pre-onset and Onset signatures for substorms in the near-tail plasma sheet: Geotail observations, *Proceedings of the Fourth International Conference on Substorms (ICS-4)*, Terra Scientific, Tokyo, p. 131, 1998.
- T. Nagai, M. Fujimoto, T. Saito, S. Machida, T. Terasawa, R. Nakamura, T. Yamamoto, T. Mukai, T. Yamamoto, A. Nishida, and S. Kokubun, Structure and dynamics of magnetic reconnection for substorm onset with Geotail observations, *J. Geophys. Res.*, 103:4419, 1998.
- K.-I. Nishikawa, Particle entry into the magnetosphere with a southward IMF as simulated by a 3-D EM particle code, *J. Geophys. Res.*, 102:17,631, 1997.
- K.-I. Nishikawa, Reconnections at near-Earth magnetotail and substorms studied by a 3-D EM particle code, in *Geospace Mass and Energy Flow: Results From the International Solar-Terrestrial Physics Program*, Geophys. Monogr. Ser., vol. 104, edited by J. L. Horwitz, W. K. Peterson, and D. L. Gallagher, p. 175, AGU Washington D.C., 1998a.
- K.-I. Nishikawa, Particle entry through reconnection grooves in the magnetopause with a dawnward IMF as simulated by a 3-D EM particle code, *Geophys. Res. Lett.*, 25:1609, 1998b.
- K.-I. Nishikawa, and S. Ohtani, Evolution of thin current sheet with a southward interplanetary magnetic field studied by a three-dimensional electromagnetic particle code, *J. Geophys. Res.*, 105, May, 2000.
- S. Ohtani, K. Takahashi, T. Higuchi, A. T. Y. Lui, H. E. Spence, and J. F. Fennell, AMPTE/CCE-SCATHA simultaneous observations of substorm-associated magnetic fluctuations, *J. Geophys. Res.*, 103:4671, 1998.
- S. Ohtani, F. Creutzberg, T. Mukai, H. Singer, A. T. Y. Lui, M. Nakamura, P. Prikyl, K. Yumoto, and G. Rostoker, Substorm onset timing: The December 31, 1995, event, *J. Geophys. Res.*, 104:22,713, 1999.
- V. A. Sergeev, V. Angelopoulos, D. G. Mitchell, and C. T. Russell, In situ observations of magnetotail reconnection prior to the onset of a small substorm, *J. Geophys. Res.*, 100:19,121, 1995.
- V. A. Sergeev, K. Liou, C.-I. Meng, P. T. Newell, M. Brittnacher, G. Park, and G. D. Reeves, Development of auroral streamers in association with localized impulsive injections to the inner magnetotail, *Geophys. Res. Lett.*, 26:417, 1999.
- K. Shiokawa, W. Baumjohann and G. Haerendel, Braking of high-speed flows in the near-earth magnetotail. *Geophys. Res. Lett.*, 24:1179, 1997.
- K. Shiokawa, W. Baumjohann, G. Haerendel, G. Paschmann, J. F. Fennel, E. Friis-Christensen, H. Lühr, G. D. Reeves, C. T. Russell, P. R. Sutcliffe, and K. Takahashi, High-speed ion flow, substorm current wedge, and multiple Pi2 pulsations. *J. Geophys. Res.*, 103:4491, 1998a.
- K. Shiokawa, G. Haerendel, and W. Baumjohann, Azimuthal pressure gradient as driving force of substorm currents, *Geophys. Res. Lett.*, 25:959, 1998b.
- B. U. Ö. Sonnerup, Magnetic field reconnection, in *Solar System Physics, Vol. III*, edited by T. L. Lanzerotti, C. F. Kennel, and E. N. Parker, p. 45, North-Holland, Amsterdam, 1979.
- T. Terasawa, Hall current effect on tearing mode instability, *Geophys. Res. Lett.*, 10:475, 1983.
- J. Villasenor, and O. Buneman, Rigorous charge conservation for local electromagnetic field solvers, *Comp. Phys. Comm.*, 69:306, 1992.